Aerodynamic study of a suspension bridge deck by CFD simulations, wind tunnel tests and full-scale observations

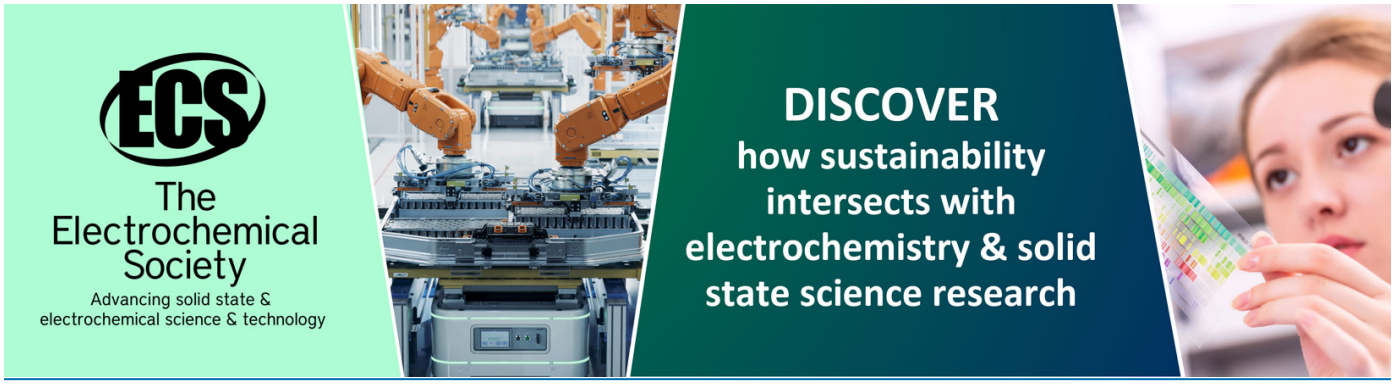

Aerodynamic study of a suspension bridge deck by CFD simulations, wind tunnel tests and full-scale observations

I. Kusano[1]*, E. Cheynet[2], J. B. Jakobsen[3] and J. Snæbjörnsson[4]

[1]School of Industrial Engineering, IQS Universitat Ramon Llull, Via Augusta, [3]90, Barcelona Spain
[2]Bergen Offshore Wind Centre and Geophysical Institute, University of Bergen, Bergen, Norway
[3]Dept. Mechanical and Structural Engineering and Material Science, University of Stavanger, Kjell Arholmsgate 41, Stavanger, Norway
[4]Department of Engineering, Reykjavik University, Menntavegur 1 IS-101, Reykjavík, Iceland

E-mail: ibuki.kusano@iqs.url.edu

Abstract. Assessing the aerodynamic characteristics of long-span bridges is fundamental for their design. Depending on the terrain complexity and local wind conditions, episodes of large angles of attack (AoA) of 15° may be observed. However, such large AoAs (above 10°) are often overlooked in the design process. This paper studies the aerodynamics properties of a flow around a single-box girder for a wide range of AoAs, from −20° to 20°, using numerical simulations. The simulations are based on a 2D unsteady Reynolds-averaged Navier–Stokes (URANS) approach using the $k-\omega$ SST turbulence model with a Reynolds number of 1.6×10^5. Numerically obtained aerodynamic static coefficients were compared to wind tunnel test data. The CFD results were generally in good agreement with the wind tunnel tests, especially for small AoAs and positive AoAs. More discrepancies were observed for large negative AoA, likely due to the limitation of modelling 3D railings with 2D simulations. The simulated velocity deficit downstream of the deck was consistent with the one measured in full-scale using short-range Doppler wind lidar instruments. Finally, the Strouhal number from the CFD simulations were in agreement with the value obtained from the full-scale data.

1. Introduction

Wind turbulence plays an important role in the structural behaviour of long-span suspension bridges [1, 2]. Depending on the wind conditions and geographical features of bridge locations, there may be episodes of incoming winds with large angles of attack (AoAs) up to 15°or more. This is for instance the case for the Lysefjord Bridge in Norway where the ratio of the vertical turbulent intensity I_w over the longitudinal one I_u was found to range from 0.6 to 0.7, which is much higher than in flat terrains [3, 4]. The large ratio implies that the instantaneous angle of attack could reach values above 20°.

However, such large angles of attack are often overlooked in design, and wind tunnel tests are typically carried out in the range of ±10°. Recent studies [5, 6] have shown that the instantaneous AoAs can have a significant influence on the non-linear turbulent loading. In this regard, a reassessment of the aerodynamic coefficients of a bridge deck at large AoAs is necessary for the safe design of long-span bridges in complex terrains, where large AoAs can be observed.

The characterization of the aerodynamic response of a bridge girder has historically been performed in wind tunnel tests. However, with the rapid advances in readily available computational power and numerical methods, the use of Computational Fluid Dynamics (CFD) has become increasingly reliable for the last two decades, see e.g. [7, 8, 9].

The objective of this study is to investigate the aerodynamic behaviour of the deck of a suspension bridge at large angles of attack using Computational Fluid Dynamics (CFD) simulations. Key results from the CFD simulations, i.e., the aerodynamic force coefficients and the Strouhal number, are compared to results from recent sectional model tests of the Lysefjord bridge [10]. Once the CFD models are validated through comparison with the wind tunnel tests, some flow field characteristics from the CFD analyses are compared to available full-scale wind data from a previous lidar campaign on the same bridge [11]. The aim is to show the complementary relevance of the CFD method to full-scale and wind-tunnel measurements.

2. Theoretical background

2.1. Flow model

The flow around the deck section is modelled using the Unsteady Reynolds-Averaged Navier Stokes (URANS) equations, which are derived from the Navier-Stokes equations with a turbulent stress tensor [12].

$$\frac{\partial U_i}{\partial x_i} = 0 \tag{1}$$

$$\rho\frac{\partial U_i}{\partial t} + \rho U_j\frac{\partial U_i}{\partial x_j} = -\frac{\partial P}{\partial x_i} + \frac{\partial}{\partial x_j}\left(2\mu S_{ij} + \rho\tau_{ij}\right) \tag{2}$$

where U_i is the vector of mean velocity, x_i is the position vector, ρ is the fluid density, t is time, P is mean pressure, μ is molecular viscosity, S_{ij} is the mean strain-rate tensor and τ_{ij} is the specific Reynolds stress tensor defined as

$$\tau_{ij} = -\overline{u_i' u_j'} \tag{3}$$

where u_i' is the vector of fluctuating velocity.

Different URANS formulas can be obtained depending on the turbulence model selected. The $k-\omega$ Shear Stress Transport (SST) turbulence model [13], which is widely used in the bridge engineering community, was selected among many available turbulence models to investigate the flow around the deck in this study. It is known to be well suited to study complex flow with adverse pressure gradients capturing realistically regions of flow recirculation and separation. See for example [14, 15, 16, 17].

2.2. Force coefficients

The aerodynamic force coefficients and Strouhal number of a bridge deck section under wind load are defined as:

$$C_L = \frac{L}{0.5\rho U^2 B};\ C_D = \frac{D}{0.5\rho U^2 H};\ C_M = \frac{M}{0.5\rho U^2 B^2};\ S_t = \frac{fH}{U} \tag{4}$$

where C_L, C_D and C_M are lift, drag and moment coefficients, respectively; L, D and M are the time-averaged lift and drag forces and moment per unit of length, ρ is the fluid density, U is the undisturbed mean wind speed, f is the vortex shedding frequency and B and H are the width and the height of the deck cross-section, respectively. The force and sign convention used for

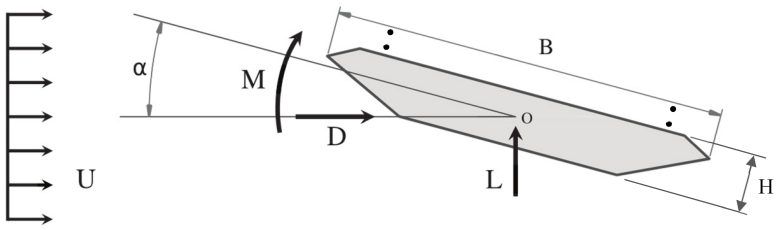

Figure 1. Force and sign convention of a bridge deck under constant velocity. The AoA is denoted α and depends on both the rotational motion of the deck and non-horizontal flow characteristics.

the study is shown in fig. 1. The drag coefficient of the deck can also be estimated using the conservation of momentum and the velocity deficit downstream of the bridge [11] as:

$$C_D = \frac{2}{H\overline{u}_0} \int_{z_1}^{z_2} [\overline{u}_0 - \overline{u}(z)]\, \mathrm{d}z \tag{5}$$

Here H is the deck height, is the undisturbed mean wind velocity, z_1 and z_2 are two vertical reference locations in the wake such that $z_2 - z_1$ represents the width of the wake.

3. CFD analysis of the bridge deck

3.1. Geometry and computational modelling

The Lysefjord bridge is a long-span suspension bridge located in Rogaland, Norway. Its main span is 446 m and the concrete tower is 102 m high. The steel deck is 12.3 m wide and 2.7 m deep with two traffic lanes and a pedestrian lane as shown in the left panel of fig. 2.

CFD simulations were conducted based on a 1:50 scale of the bridge deck, which was also adopted for the recent sectional model tests of the deck in the wind tunnel. The bridge deck has three sets of circular railings (See fig. 2). The two outer railings are composed of a continuous horizontal section supported by vertical bars every 0.14 m. To model the influence of the vertical bars on the flow in the 2D model, two smaller circular sections were added, with an equivalent wind projected area.

The simulations were performed to obtain the force coefficients of the bridge deck at different angles of attack as well as velocity and pressure in several virtual probe points within the fluid domain. A 2D URANS approach was adopted to perform the analyses using the open-source CFD code of OpenFOAM v.6.0 [18]. Three-dimensional approaches such as 3D detached Eddie Simulations or Large Eddy Simulations were not considered in this study because of their high computational cost. Said differently, the 2D approach was adopted here to assess how a cost-effective engineering tool can complement wind tunnel tests and full-scale measurements for the study of aerodynamic coefficients of a bridge deck in complex terrain.

The flow domain and the boundary conditions used for the study are illustrated in fig. 2 (right). A flow domain of 36B x 26B is adopted where B is the width of the deck. A constant inlet velocity of 10 $\mathrm{m\,s^{-1}}$ was applied at the upwind boundary with a turbulent intensity of 12%. This turbulent intensity value is consistent with the one measured during the Lysefjord Bridge wake study by Doppler wind lidars in 2014 [11]. Atmospheric pressure was imposed at the outlet boundary. The upper and lower boundaries were defined as slip walls while the deck and railing contours were defined as non-slip walls.

A linear scheme was used for the interpolation from cell to face centres, and the gradient terms are discretized using the Gauss scheme with linear interpolation scheme. The Gauss scheme is

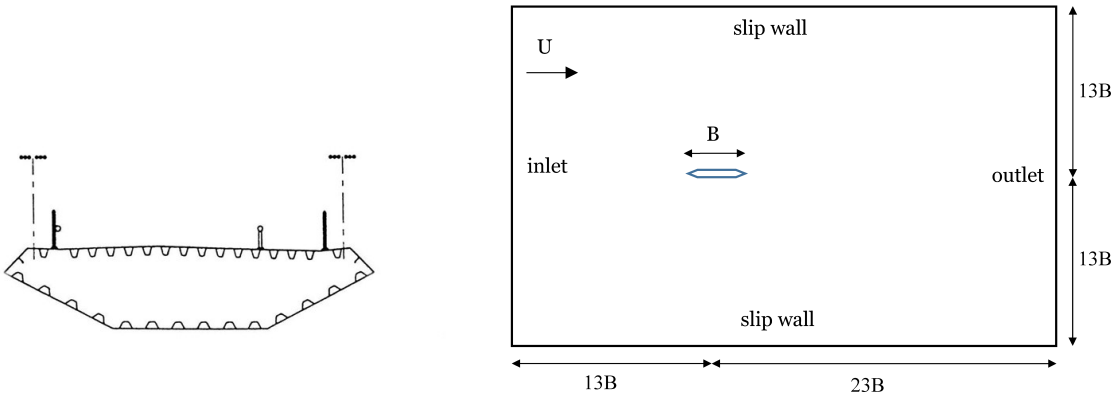

Figure 2. the cross section of the bridge (left) and the flow domain and the boundary conditions (right).

also used for the divergence terms with linear upwind and limited interpolations schemes. Finally, the discretization in time was done by a Forward Euler scheme. The pressure-velocity coupling was solved by the PIMPLE algorithm, where both outer and inner correctors are set to 2. The residual tolerance of for U and P was set to 1×10^{-5} and 1×10^{-4}, respectively.

A boundary layer mesh was applied using the software Pointwise around the deck and the railings. The boundary layer mesh size was limited to a maximum y^+ value less than 4, which was the maximum value from all simulations. The y^+ value is defined as:

$$y^+ = \frac{u_* y}{\nu} = \sqrt{\frac{\tau_w}{\rho}} \frac{y}{\nu} \tag{6}$$

where u_* is the wall friction velocity; y is the distance from the wall to the first cell centre; τ_w is the wall shear stress and ν is the local kinematic viscosity of the fluid.

The first element height was set to $y/B = 2.03 \times 10^{-4}$ and the Courant number was set to 1 for simulation with a mean non-dimensional time step, $\Delta s = \Delta t U/B = 1.2 \times 10^{-4}$. Prior to the study, the time integration was verified by comparing the results with Courant numbers 1 and 0.5, and no significant difference was found. The total simulation time was 5 seconds, which in full scale, correspond to 250 seconds. The total CPU time for the zero degree AoA was 237 hours, using 20 CPUs in parallel and a time step of ca. 3×10^{-6} s. It should be noted, that the computational time partly depends on the sampling frequency used for data extraction. Using a lower sampling frequency will reduce the CPU time.

A mesh convergence study was conducted with three different mesh densities for 0° angle of attack. Three types of meshes were considered: a coarse mesh with 180,237 cells, a medium-mesh with 259,151 cells and a fine mesh with 312,448 cells. Since the fine and the medium meshes gave similar results while the coarse mesh underestimated the lift coefficient, the medium mesh scheme was chosen for the simulations.

Figure 3 shows the mesh used for the study including the details around the deck and the railings. The unstructured mesh was used due to the complexity of the geometry with the railings around the deck. CFD simulations were carried out for 11 angles of attack, from -20° to +20°every 4° to investigate the static aerodynamic force coefficients.

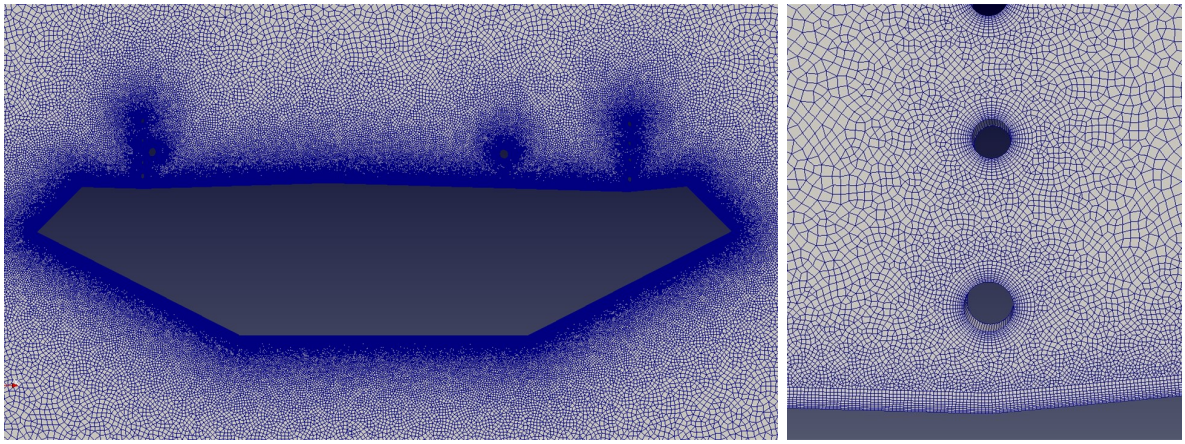

Figure 3. Mesh of the deck with detail of the railings and the boundary layers.

3.2. CFD results

Figure 4 depicts the instantaneous flow fields of pressure (top) and horizontal velocity (bottom) for AoA of 0°, +20° and -20°. The pressure is plotted between -30 Pa and 30 Pa for the clarity of visualization in the flow field. As can be seen, large vortices are formed in the downstream region for large angles of attack. For -20° AoA, a positive pressure is observed on the top half of the deck and the rest of the deck is under negative pressure. High velocities occur where the flow passes the last set of railings, and negative velocities are associated with vortices formed under and behind the deck as well as behind the railings. For +20° AoA, a negative pressure is visible all around the deck except for the lower side edge facing the incoming flow. For 0° AoA, a large negative pressure is produced behind the first set of railings.

Instantaneous streamlines are displayed in fig. 5. For -20°, large alternating vortices are shed from the three bottom surfaces of the deck. For +20°, besides the alternating vortices, smaller vortices are formed behind the railings on the top surface. For an AoA of 0°, the vortex shedding process is primarily confined to the near wake area defined by the deck height.

Figure 6 shows the time histories of the force coefficients (top panels) and the power spectral densities (PSDs) of lift coefficient (bottom panels). Table 1 lists the coefficient values, their standard deviations, denoted σ_i, where $i = C_D, C_L, C_M$, and the Strouhal number for each AoA.

For an AoA of 0°, the lift coefficient exhibits a wide range of frequencies with a relatively small standard deviation of 0.028. On the other hand, the lift coefficients for large angles show large standard deviations, 0.20 for -20° and 0.18 for +20°, which are six to seven times larger than for 0°. The PSDs also exhibit a clear frequency peak near 19.2 Hz for -20° and 22.0 Hz for +20°. The large, harmonic lift fluctuations at the angles of attack of +20° and -20° are associated with the vortex shedding processes encompassing the entire lower/upper part of the deck, as illustrated in fig. 5. Such a flow separation along an entire "lifting surface" is known as the stalling condition. The Strouhal number for an AoA of 0° was calculated based on the centre of the broadband frequency whose value was 0.135.

3.3. Experimental validation of the CFD models

The force coefficients obtained at different angles of attack with the CFD simulations are compared to those from recent static wind tunnel tests, performed on a 1/50 scale section model of the Lysefjord bridge deck [10]. The section model had a width of 0.246 m and a length of 2.4 m respectively, whereas the wind tunnel section was 2.4 m by 3m. The reference mean wind speed was 10 $\mathrm{m\,s^{-1}}$ and the turbulent intensity at the bridge height was 10%. Six load sensors were used to measure the drag force, lift force and torsional moment.

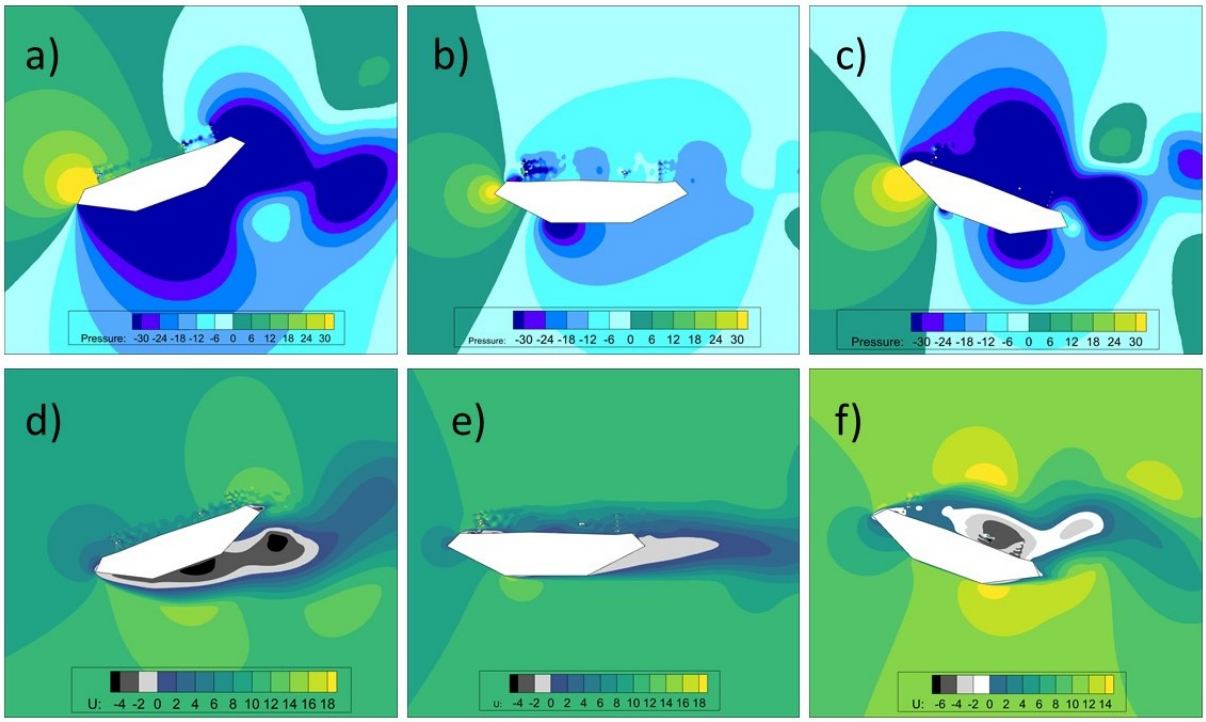

Figure 4. Instantaneous flow fields of -20°, 0° and +20° AoA: (a)-(c) pressure (Pa) (d)-(f) horizontal velocity ($\mathrm{m\,s^{-1}}$).

Table 1. Summary of force coefficients, standard deviations, and St. number from CFD simulations.

AoA	C_D	C_L	C_M	σ_{C_D}	σ_{C_L}	σ_{C_M}	St
-20	2.674	-1.034	-0.132	0.158	0.205	0.028	0.103
0	0.814	-0.064	0.041	0.024	0.028	0.005	0.135
20	1.670	0.339	0.184	0.079	0.184	0.025	0.119

The results of the CFD simulations are illustrated along with the experimental data in fig. 7. In general, the simulations trace well the experimental results between -4° and +16°, but for negative angles beyond -4°, especially at -8° and -12°, the simulations overestimate all coefficients. For an AoA of -8° and -12°, The simulated coefficients CD, CL and CM are overestimated by 50%, 32% and 25% respectively. This may reflect the need to model the railings in a more realistic manner for the negative AoAs, since the railings produce a turbulent wake that interacts with the flow on the upper side of the deck. The 2D simulation models in this study cannot account accurately for the 3D geometry of the railings although some corrections were made in the model (Section 3.1). This further reminds that 3D flow effects become important at large AoAs. In general, the CFD and the experimental results match well for the positive angles although, for the AoA of +20°, the CFD analysis slightly overestimates CD while underestimating CL. Another source of discrepancy could be the difference in the two blockage ratios. For the largest angles of attack, the wind-exposed dimension of the section model was about 3.5% of the test section height, while the blockage ratio in the simulations was approximately half of that value. The overall blockage levels were limited and their difference in the experimental and numerical

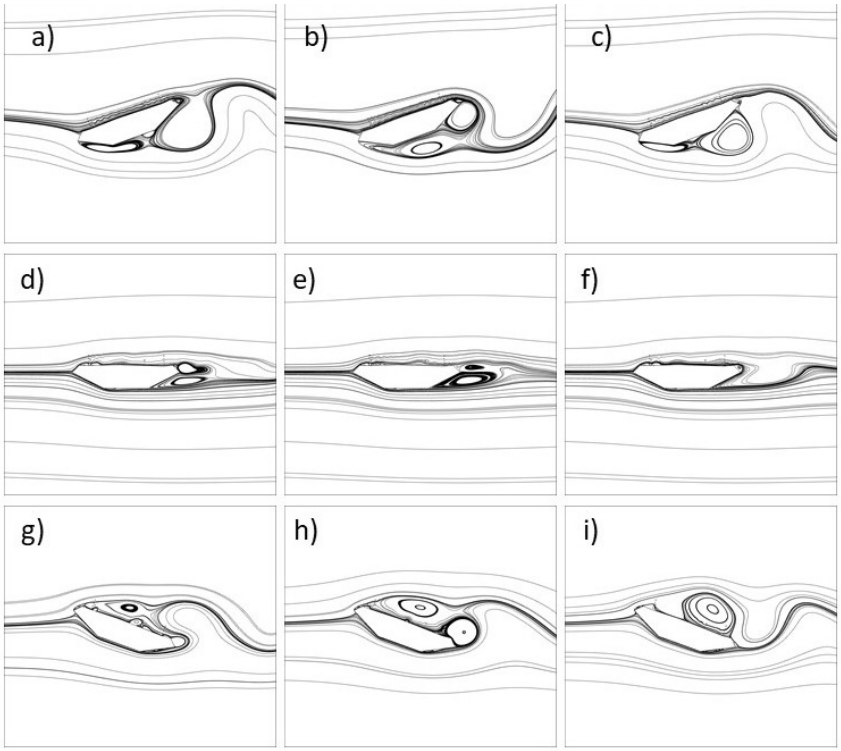

Figure 5. Streamlines of instantaneous flow fields: for -20° AoA: a) tU_∞/H= 505.6, b) tU_∞/H= 509.3 c) tU_∞/H= 513.0; for 0° AoA: d) tU_∞/H= 838.9, e) tU_∞/H= 840.7 f) tU_∞/H= 842.6; for +20° AoA:g) tU_∞/H= 922.2, h) tU_∞/H= 924.1 i) tU_∞/H= 925.9.

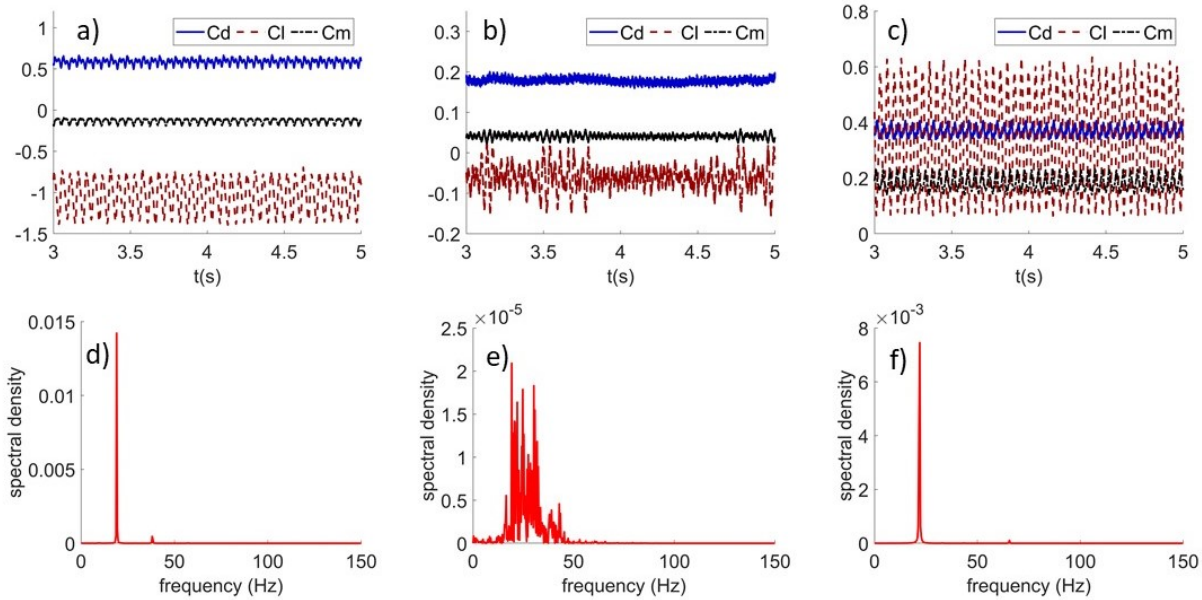

Figure 6. Force coefficients time history (top panels) and the spectral density of CL (bottom panels): for (a) and (d) -20° AoA, (b) and (e) 0° AoA, and (c) and (f) +20° AoA.

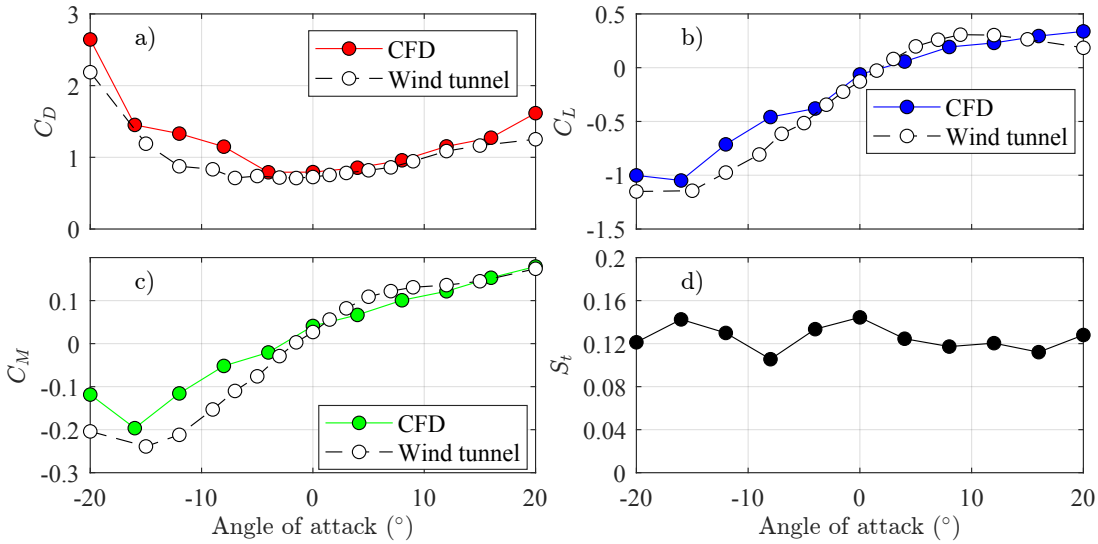

Figure 7. Aerodynamic parameters as a function of the angle of attack: time-averaged (a) drag coefficient , (b) lift coefficient, (c) moment coefficient and (d) Strouhal number .

simulations is expected to be of secondary importance for the sharp-edged section studied.

Strouhal number does not vary much when varying the AoA. The decreasing Strouhal number for large negative and positive angles of attack is understood to be associated with the increasing projection area to the incoming flow due to the large AoA. According to the buffeting theory, which is used to study the dynamic response of bridge decks to incoming turbulence, the lateral response is positively correlated with the drag coefficient and negatively correlated with the lift coefficient. At large AoAs, the lift coefficient becomes almost constant and even decreases for the AoA above 15°. Therefore, the attenuation effect due to the lift coefficient becomes weaker at large AoAs. The weakening of this attenuation effect is not predicted by the linear buffeting theory. In complex terrain, where the vertical turbulence intensity is relatively high, the instantaneous AoAs can be larger than 15°. In such an environment, the dynamic lateral bridge response may, therefore, be considerably larger than predicted by the linear buffeting theory, as observed on the Lysefjord Bridge [19]. Even though the large AoAs measured from a bridge deck are only instantaneous values, studies by [5, 6] indicate that non-linear buffeting forces can result from fluctuating AoA.

4. Comparison of the CFD simulations with full-scale measurements

4.1. Full-scale wind measurement downstream of the bridge deck

Validation of wind tunnel and numerical flow simulations of bridge aerodynamics by measurements in full scale has been limited due to the complexity of such measurements. This also includes the difficulties in reaching the disturbed flow regions around the bridge deck, using traditional anemometers. To bridge this gap, Cheynet et al. [11] carried out a pilot study on the applicability of lidars for assessing wind conditions at the Lysefjord bridge site. The studies documented for the first time the velocity deficit downstream of a full-scale bridge using a dual short-range Doppler wind lidar system.

The flow conditions downstream of the Lysefjord bridge deck were studied by wind lidars installed on the bridge walkway during a four-day pilot experiment [11]. The two lidars were located symmetrically at 45 m from the mid-span [11] and monitored the wind flow along a vertical line segment above and below the deck at a 3.25B distance (40 m) from the trailing edge, with a sampling period of one second. The acquired wind data were analyzed in terms of the

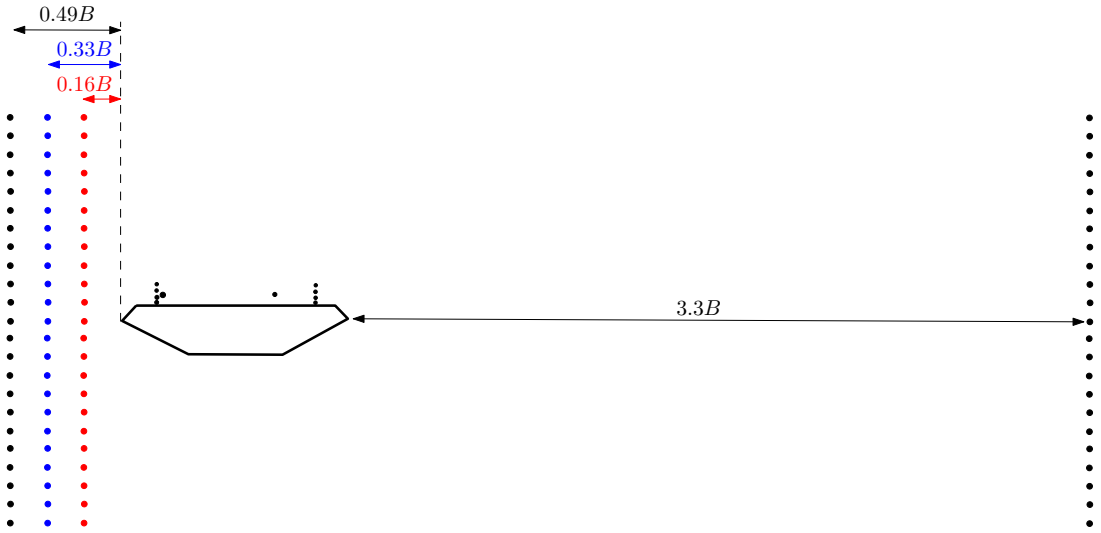

Figure 8. Side view of the virtual probe locations in the CFD model, where B is the deck width.

mean velocity, turbulence intensity and vortex shedding frequencies.

The corresponding flow conditions in the present CFD model were studied with a series of virtual probes placed vertically at the same distance downstream from the deck as in full scale as shown in fig. 8. Additionally, several virtual probes were placed upstream at distances of 0.16B, 0.33B and 0.49B away from the leading edge to see how far the upstream flow can be disturbed by the presence of the deck. The CFD model at 0° angle of attack from the previous section was used for a simulation period of 5 seconds, which correspond to a simulation period of 250 seconds in full-scale. The horizontal mean wind speed was normalized by the inlet velocity at each probe location.

The right panel of fig. 9 shows the normalized horizontal wind velocity profile at the downstream location, from the full-scale measurements and the CFD simulations. The full-scale data is based on an ensemble averaging of 18 samples of 10 min duration recorded between 04:00 to 07:50 on 23/05/2014.

The mean velocity recorded by the lidars is normalized by the undisturbed mean velocity u0 upstream to the deck, and the vertical location is normalized with the deck height H where $z/H = 0$ at the trailing edge location. The average data are displayed in a scatter plot, whose fitted curves are shown with a solid line. The vertical extent of the velocity deficit region due to the presence of the deck from the CFD simulation, 4.44H is about 25% smaller than that from the full-scale measurement data of $5.92H$. The change in velocity profile is more gradual for the full-scale measurement compared to the CFD results. Overall, the full-scale wake is "broader" and the CFD simulation overestimates the velocity deficit at $z/H = 0$, but underestimates the deficit below and above the deck. Considering the complex three-dimensional flow conditions in full-scale, as well as the contribution of main bridge cables to the observed wake conditions, the overall agreement between the two wind profiles is judged satisfactory.

The simulated normalized average velocity on the upstream side of the deck are expressed as a function of the normalized z location, z/H in the panel b of fig. 9). No full-scale data is available at this location. For the set of the virtual probes nearest to the deck ($0.16B$), the flow disturbance is obviously larger, but the probes vertically away from the deck indicates the average velocity returns to the undisturbed one faster than the more upstream locations, at $0.33B$ and $0.49B$.

The Strouhal number computed from the full-scale measurements was 0.10, which was lower

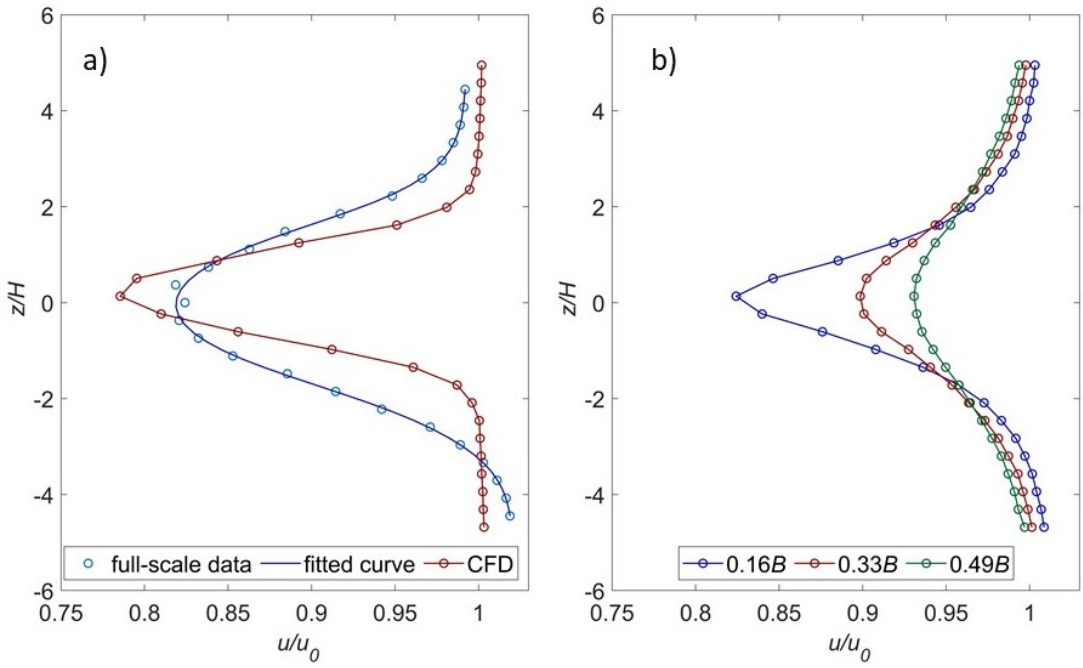

Figure 9. Panel (a): Normalized mean wind speed downstream of the deck at a distance of $3.25B$ from the trailing edge expressed as a function of the distance to the trailing edge. Averaged full-scale data are displayed as a blue scatter plot: the solid blue line smooths the scattered data using a piecewise cubic spline. Panel (b): normalized mean wind speed upstream of the deck at a distance of $0.16B$, $0.33B$ and $0.49B$ from the leading edge.

than the CFD results of 0.14. As mentioned in the previous section, the Strouhal number computed from the CFD simulation was based on the broad-banded spectral peak, and the lower end of the frequency is associated with the Strouhal number close to this full-scale value.

The drag coefficient was also estimated using eq. (5) and the data set shown in fig. 9. The design drag coefficient of the Lysefjord bridge is 1.0 [11]. The C_D value from the full-scale measurements ranged from 1.0 and 1.1, which was slightly larger than the CD computed based on the CFD data of 0.9. It is also larger than the time-averaged C_D from the CFD simulations, 0.8, or from the experimental result of 0.7 in the previous section. According to Zu et al. [20], the drag coefficients reduces slightly with the yaw angle, which ranged from 20° to 30° in [11]. Therefore, the larger CD value found in full-scale is considered to be due to the presence of the main cables a few meters above the deck at mid-span, which increases the drag force.

5. Conclusions

The study of the aerodynamic properties of a long-span suspension bridge deck was carried out using computational fluid dynamic (CFD) simulations, experimental tests, and full-scale measurement data. The flow simulation was conducted using the 2D Unsteady Reynolds-Averaged Navier Stokes method with the $k-\omega$ SST turbulence model at $Re = 1.6 \times 10^5$ for a wide range of angles of attack (AoAs) from -20° to 20°. For a more realistic study of the flow around the girder, the railing of the deck was included in the geometry. The time-averaged values of the aerodynamic force coefficients were compared to the wind tunnel tests data. The CFD results show an overall good agreement with the experimental data, especially for low positive AoAs. The static aerodynamic coefficients were overestimated for negative AoAs with values larger than $-8°$ due to the limitation of modelling 3D railing effects in 2D simulations and the

possible interaction between the railing-induced wake and upper deck level. For large AoAs, large oscillating vortices are formed on the downstream side of the deck.

The simulated mean wind velocity profile downstream of the deck was compared with the full-scale measurement data collected by a dual short-range wind lidar system at a distance equal to 3.3 times the deck width. The simulated wake was narrower than observed by the lidar instruments, and the CFD simulation overestimated slightly the mean velocity deficit at the deck level. An alternative method to estimate the drag coefficient was conducted using the vertical wind speed profile downstream of the deck. The CFD data was consistent with the full-scale measurements considering the presence of the main cable, which is located 4 m above the bridge deck.

The present results show that, although 2D simulations have their own limitations, they may provide reasonably good and fast estimates of the aerodynamic coefficients, especially for small AoAs. Therefore, it is an efficient tool for the initial design phase of a bridge deck or when no wind tunnel test is available.

References

[1] Davenport A G 1961 *Proceedings of the Institution of Civil Engineers* **19** 449–472
[2] Scanlan R 1978 *Journal of Sound and vibration* **60** 201–211
[3] Solari G and Piccardo G 2001 *Probabilistic Engineering Mechanics* **16** 73–86
[4] Cheynet E, Jakobsen J B and Snæbjörnsson J 2019 *Journal of Sound and Vibration* **450** 214–230
[5] Argentini T, Rocchi D and Somaschini C 2020 *Journal of Wind Engineering and Industrial Aerodynamics* **197** 104072
[6] Diana G and Omarini S 2020 *Journal of Wind Engineering and Industrial Aerodynamics* **201** 104163
[7] Mannini C, Šoda A, Voß R and Schewe G 2010 *Journal of Wind Engineering and Industrial Aerodynamics* **98** 742–753
[8] Šarkić A, Fisch R, Höffer R and Bletzinger K U 2012 *Journal of Wind Engineering and Industrial Aerodynamics* **104** 141–151
[9] Ge Y and Xiang H 2008 *Journal of Wind Engineering and Industrial Aerodynamics* **96** 1912–1924
[10] SOH Wind Engineering 2021 Lysefjord Bridge, Norway. Static wind tunnel tests
[11] Cheynet E, Jakobsen J B, Snæbjörnsson J, Angelou N, Mikkelsen T, Sjöholm M and Svardal B 2017 *Journal of Wind Engineering and Industrial Aerodynamics* **171** 261–272
[12] Wilcox D 2006 *Turbulence Modeling for CFD* (Third ed. DCW ind. Inc, La Canada, CA, USA.) ISBN 9781928729099
[13] Menter F and Esch T 2001 *16th Brazilian Congress of Mechanical Engineering (COBEM)* vol 109 p 650
[14] Nieto F, Hargreaves D, Owen J S and Hernández S 2015 *Engineering Applications of Computational Fluid Mechanics* **9** 157–173
[15] Álvarez A, Nieto F, Kwok K and Hernández S 2018 *Journal of Wind Engineering and Industrial Aerodynamics* **182** 202–221
[16] Jeong W, Liu S, Bogunovic Jakobsen J and Ong M C 2019 *Energies* **12** 2670
[17] Montoya M C, Nieto F, Hernández S, Kusano I, Álvarez A and Jurado J 2018 *Journal of Wind Engineering and Industrial Aerodynamics* **177** 405–428
[18] Weller H, Tabor G, Jasak H and Fureby C 1998 *Computers in Physics* **12** 620–631
[19] Cheynet E, Jakobsen J B and Snæbjörnsson J 2016 *Engineering Structures* **128** 474–487
[20] Zhu L, Xu Y L, Zhang F and Xiang H 2002 *Journal of Wind Engineering and Industrial Aerodynamics* **90** 781–805